JAAS

ROYAL SOCIETY OF CHEMISTRY

PAPER

View Article Online
View Journal | View Issue

Cite this: *J. Anal. At. Spectrom.*, 2025, **40**, 2692

SI-traceable total analysis of nitrate and nitrite by isotope dilution optical spectroscopy and its application to Berlin surface waters

Carlos Abad, *[a] Dennis Jegielka,[ab] Allen Aloysius[ac] and Sebastian Recknagel [a]

Accurate nitrate and nitrite data support water-quality regulation, yet routine methods rely on external calibration and rarely achieve SI traceability. We report a calibration-free determination of nitrate and nitrite by combining isotope dilution with high-resolution continuum-source graphite furnace molecular absorption spectrometry (ID-HR-CS-GF-MAS). A ^{15}N-enriched nitrate spike (its concentration verified by reverse isotope dilution against the standard reference material NIST 3185) provides the SI link, and it is gravimetrically added to samples; nitrate and residual nitrite are converted in situ to nitric oxide (NO), whose 215 nm band is recorded at a pixel resolution of $\lambda/\Delta\lambda \approx 140\,000$. The 0.2127 nm shift between ^{14}NO and ^{15}NO electronic spectra is resolved, and a three-latent-variable partial least squares regression model yields the $^{15}N/^{14}N$ ratio with 0.3% precision. Instrumental LoD values of 4.8 ng (^{14}N) and 3.2 ng (^{15}N) translate to a method LoD of 4.8 ng of nitrogen (equivalent to 1.05 mg L^{-1} NO_3^- for a 20 µL aliquot). The furnace program allows for successive drying/pyrolysis loops, so additional 20 µL aliquots can be layered onto the graphite platform. Alternatively, a 10 mL anion-exchange solid-phase extraction step concentrates nitrate and nitrite fivefold, allowing for the analysis of even lower sample concentrations. Results for four certified reference materials (2.9 to 1000 mg L^{-1} NO_3^-) agreed with certified values, giving relative expanded uncertainties of 2 to 4%. Analysis of twenty Berlin surface-water samples revealed concentrations ranging from 0.10 to 7.3 mg L^{-1} NO_3^-, indicating that the Panke River and Teltow Canal are the primary sources of nitrogen. ID-HR-CS-GF-MAS thus delivers ID-MS-level accuracy in a few minutes per run with bench-top optics, and, with optional on-platform or SPE pre-concentration, extends SI-traceable nitrate/nitrite monitoring into the low-ng regime.

Received 30th June 2025
Accepted 29th July 2025

DOI: 10.1039/d5ja00252d

rsc.li/jaas

1. Introduction

Nitrate and nitrite are critical water-quality indicators: essential nutrients at low levels, but at high concentrations they pollute aquatic systems and threaten human health.[1,2] Nitrate in drinking water is strictly regulated, with levels that should not exceed 10 mg L^{-1} (measured as nitrogen) by U.S. and European regulations.[3,4] Above this level, ingestion can dominate an infant's nitrate intake (≈8 to 9 mg kg^{-1} day^{-1} for bottle-fed babies). In natural waters, excess nitrate and nitrite drives eutrophication, algal blooms, and oxygen depletion, disrupting ecosystems.[5] Monitoring nitrate and nitrite with high accuracy is therefore critical for environmental protection and public health.[6]

Conventional nitrate and nitrite analysis (*e.g.*, ion chromatography) relies on external calibration and is not inherently SI-traceable.[7,8] By contrast, isotope-dilution (ID) is an absolute analytical method that yields directly SI-traceable results.[9,10] ID-mass-spectrometry (ID-MS) has demonstrated this for nitrate with 2–5% precision, but such methods require complex sample preparation and expensive instrumentation.[10] There is thus a need for simpler, absolute methods, especially ID approaches, for quantifying nitrate and nitrite, and optical spectroscopy provides an alternative.

High-resolution continuum-source molecular absorption spectrometry (HR-CS-MAS) has emerged as a powerful optical technique for non-metal analytes. A continuum lamp that covers the 190–900 nm range is combined with a high-resolution spectrometer. This setup visualizes the bands of diatomic molecules and significantly reduces spectral interference.[11]

Recent advances have opened the door to isotopic analyses *via* molecular absorption, combining the strengths of ID with the convenience of optical detection.[12,13] The fundamental principle enabling this combination is the isotopic shift, where isotopologues of a diatomic molecule absorb at slightly

[a]*Bundesanstalt für Materialforschung und -prüfung (BAM), Division Inorganic Reference Materials, Richard-Willstätter-Str. 11, 12489 Berlin, Germany. E-mail: Carlos.Abad@bam.de*

[b]*Humboldt Universität zu Berlin, Department of Chemistry, Brook-Taylor-Str. 2, 12489 Berlin, Germany*

[c]*Freie Universität Berlin, Institute of Chemistry and Biochemistry, Arnimallee 22, 14195 Berlin, Germany*

different wavelengths due to mass-dependent shifts in their rotational–vibrational energy levels. In general, these shifts are more pronounced for molecular spectra than for atomic spectra, which is advantageous for optical resolution of isotopic signals. Over the past decade, it has capitalized on this by implementing ID with HR-CS-GF-MAS for several elements. For example, trace chlorine has been quantified by generating AlCl in a graphite furnace and measuring the absorption of $Al^{35}Cl$ and $Al^{37}Cl$ isotopologues, with an enriched ^{37}Cl spike added to the sample.[12] Similar molecular strategies have been applied to bromine,[13] calcium,[14] strontium,[15] boron,[16] and *via* the isotope shift of the main resonance atomic lines for lithium.[17] Moreover, this optical spectrometer, when combined with chemometric data analysis, has been successfully used to determine precise isotope amount ratios of boron[18] and lithium.[19,20] These studies established that HR-CS-spectrometry can indeed discern isotopic absorption features. Nitrogen falls into this category with its two stable isotopes (^{14}N and ^{15}N), making it an ideal candidate for an optical isotope dilution approach.

Notably, nitric oxide (NO) exhibits sharp UV absorption bands (around 200–250 nm) that can be generated from nitrate and nitrite.[21] Huang *et al.*[22] pioneered the HR-CS-MAS detection of NO, where they thermally decomposed nitrate in a graphite furnace. They recorded NO's UV spectrum around the 215.360 nm absorption line in a flame and a graphite furnace. They achieved a detection limit for N of 5 ng and demonstrated linearity up to 3000 ng with a graphite furnace, validating their results against certified nitrate standards. Huang also demonstrated that coexisting acids and metal ions (HCl, H_2SO_4, H_3PO_4, Fe, Cu, *etc.*) can suppress NO absorbance; however, this effect can be mitigated by using a low pyrolysis temperature. Brandao *et al.* extended NO detection to nitrite,[23,24] reducing nitrite with ascorbic acid to produce NO and measuring its absorption. This chemical-generation method achieved sub-μg mL^{-1} detection limits. Additionally, Brandao *et al.* demonstrated, using a graphite furnace, that by co-injecting HCl and tuning furnace temperatures, the nitrite signal could be thermally suppressed while nitrate yields NO. In that mode, nitrate/nitrite is quantified as total nitrate (with nitrite oxidation by H_2O_2).

Despite these advances, nitrate and nitrite have never been quantified by isotope-dilution HR-CS spectrometry. Previous optical studies relied on external or standard-addition calibration, leaving an unmet need for a fully SI-traceable, calibration-free method. In principle, the resolution of modern HR-CS instruments is sufficient to separate the 0.21 nm shift between ^{14}NO and ^{15}NO; thus, if a ^{15}N-enriched nitrate spike is added to the sample, the $^{15}NO/^{14}NO$ absorbance ratio should yield the analyte amount without recourse to a conventional calibration curve. Implementing such an optical ID scheme would provide the metrological rigor of ID-MS while retaining the simplicity, speed, and cost advantages of molecular absorption spectrometry.[25]

The present study, therefore, develops an ID-HR-CS-GF-MAS method for total nitrate/nitrite. We (i) generate NO *in situ* from nitrate and nitrite in a graphite furnace, (ii) resolve the isotopologues lines with a continuum-source echelle spectrograph, and (iii) extract the isotope ratio by multivariate regression. The work describes the optimization of furnace conditions, chemometric treatment of the spectra, and the construction of an SI-traceable measurement chain based on a gravimetrically characterized ^{15}N spike. By addressing these elements, we aim to demonstrate a practical, primary-method alternative to ID-MS for the accurate determination of nitrate and nitrite in environmental waters.

2. Experimental part

2.1 Materials

Ultrapure water (18.2 MΩ cm, Milli-Q, Millipore) was used throughout. Enriched $Na^{14}NO_3$ (99.95 atom% ^{14}N, Sigma-Aldrich) and $Na^{15}NO_3$ (>98 atom% ^{15}N, Sigma-Aldrich) served as calibration and spike sources. Calcium chloride tetrahydrate (Suprapur, Merck) was used to prepare a 1% w/v Ca modifier. High-purity argon (Ar 5.0, Air Liquide) was used as the furnace purge gas. A $NaNO_3$ solution (Suprapur, Merck) was used to optimize the measurement parameters.

Certified reference materials (CRMs) used for validation were NIST SRM 3185 (nitrate solution), a Merck nitrate CRM, River-Water-Anions CRM LGC6020 (LGC Standards, United Kingdom), and river water sample RM NWMISSIPPI-14 (Environment and Climate Change Canada, Canada); their certified values are listed in Table 1 of the Results section. The NIST SRM 3185 was also used for the traceable concentration characterization of the ^{15}N spike by gravimetric reverse isotope dilution.

2.2 Instruments and optimization of measurement parameters

NO spectral analysis was performed on a hybrid high-resolution continuum-source system that combines a commercial graphite furnace HR-CS-AAS (contrAA 800, Analytik Jena, Germany) with the MOdular Echelle Spectrograph, MOSES (Leibniz-ISAS, Berlin).[26,27] The contrAA 800 supplies (i) furnace control, (ii) a transversely heated, pyrolytically coated graphite tube with integrated platform, and (iii) broadband radiation from its 300 W xenon short-arc lamp operated in hot-spot mode. The same lamp is coupled into MOSES, whose CMOS detector captures the spectrum at a reciprocal dispersion of $\lambda/\Delta\lambda \approx 140\,000$ px^{-1} over the 200–240 nm window used for NO overview.

Liquid aliquots (20 μL sample + 5 μL 1% w/v Ca modifier) were delivered by an MPE-60 autosampler (Analytik Jena, Germany). An argon purge of 2 L min^{-1} was maintained throughout the temperature program, except during atomization (flow = 0). Furnace conditions were optimized to maximize NO yield while preventing dissociation: a multistep drying/pyrolysis sequence with gentle ramps (50 °C s^{-1}) is followed by an atomization plateau at 800 °C (full heating program in Table S1). Under these conditions, the NO γ-band ($\Delta v = +1$) was recorded with an effective wavelength spacing of ~0.02 nm, providing fully resolved ^{14}NO and ^{15}NO features for isotope-dilution evaluation. For method optimization, samples were measured in four replicates; for sample analysis and chemometric model training, ten replicates were used.

Table 1 Validation of the ID-HR-CS-GF-MAS method for total nitrate/nitrite equivalent: comparison between certified and experimentally determined nitrate-N equivalent concentrations for four reference materials at five spike/probe $^{15}N:^{14}N$ ratios. U values are expanded uncertainties ($k = 2$); E_n values < 1 indicate metrological compatibility between certified and measured results

Reference material	$^{15}N:^{14}N$ ratio	NO_3^- (certified)/mg L^{-1}	U (certified)	NO_3^- (equivalent measured)/mg L^{-1}	U (measured)	E_n
NIST SRM 3185	60 : 40	1000.6	1.8	999.13	0.25	0.95
	55 : 45			998.54	0.33	1.40
	50 : 50			1001.94	0.38	0.95
	45 : 55			999.09	0.17	0.93
	40 : 60			998.58	0.55	1.62
MERCK CRM	60 : 40	886.2	22.1	877.13	0.85	0.43
	55 : 45			879.13	1.11	0.34
	50 : 50			880.27	0.81	0.28
	45 : 55			881.35	0.20	0.22
	40 : 60			876.17	0.92	0.47
LGC6020	60 : 40	28.2	1.2	24.99	2.95	1.84
	55 : 45			27.24	0.18	0.94
	50 : 50			26.97	2.21	1.22
	45 : 55			27.38	0.29	0.91
	40 : 60			27.14	0.37	1.27
NWMISSIPPI-14	60 : 40	2.93	0.23	2.76	0.09	1.24
	55 : 45			2.67	0.17	3.96
	50 : 50			3.06	0.10	0.98
	45 : 55			2.84	0.10	0.70
	40 : 60			3.11	0.12	1.69

For ID analysis, samples with low nitrogen content (less than 10 mg L^{-1} N) can utilize the pre-concentration option described in Table S1. This option involves one or more additional 20 μL injections, which are dried and pyrolyzed (steps 4a/4b) before the final atomization, thereby increasing the total mass of nitrate/nitrite. At the opposite extreme, samples that are naturally more concentrated were diluted so that the net signal corresponded to ≈10 mg L^{-1} N. In this way, the integrated absorbances of the ^{14}NO and ^{15}NO lines always fell within the linear, high-signal region of the detector, guaranteeing comparable proportional line shapes and signal-to-noise ratios for both isotopologues across all measurements.

2.3 Preparation of isotope dilution standards and spike

All calibration mixtures were prepared by gravimetric weighing of the dry, isotopically enriched nitrate salts. The indicated masses of enriched $Na^{15}NO_3$ and $Na^{14}NO_3$ were weighed to ±0.006 mg in PFA weighing boats, transferred to PFA flasks, and dissolved in ultrapure water. The total dissolution mass was recorded so that the mass fractions $w(^{15}N)$ and $w(^{14}N)$, as well as the atom-percent abundances $x(^{15}N)$ and $x(^{14}N)$, could be calculated directly from the certified nitrogen content of each salt. Eleven binary mixtures spanning nominal $^{15}N:^{14}N$ mass ratios from 0 : 1 to 1 : 0 (Table S2) provided the calibration space for the chemometric model. The concentration of the enriched salt used for spiking was verified by reverse isotope dilution against NIST SRM 3185 before each analytical batch.

2.4 Data analysis

An adapted procedure from Winckelmann *et al.* was adapted for the isotope analysis of NO.[19] Time-resolved 3D spectra recorded with the HR-CS-AAS contrAA 800 were first baseline-corrected on the instrument and then exported through Aspect CS (version 2.2.1.0, Analytik Jena). Each atomization cycle generated a stack of 450 consecutive spectra. The dataset was imported into MATLAB (R2020a, The MathWorks Inc), where the spectra from each atomization cycle were first averaged over time to produce a single profile per sample. A blank spectrum, measured under identical conditions between each sample, was then subtracted. The resulting blank-corrected spectra were subsequently analyzed using Solo MIA software version 9.3 (Eigenvector Research, Inc., USA, 2025) to evaluate isotope amount ratios *via* the SIMPLS algorithm for partial least squares regression (PLS-R). The optimization parameters are summarized in Table S3, along with their corresponding workflow, as shown in Fig. S1.

Because only a small spectral region was sufficient for analysis, data were acquired using the commercial contrAA 800 HR-CS-AAS instrument. For every furnace cycle, the detector delivered a 200-point segment from 215.155 to 215.450 nm, around the $\Delta v = +1$ ^{14}NO band head. Each spectrum was area-normalized to remove lamp-intensity drift, converted to an 11-point, second order Savitzky–Golay second derivative to sharpen the highly overlapped rotational structure, and finally mean-centered.

The calibration matrix comprised 110 spectra: eleven gravimetric $^{15}N:^{14}N$ mixtures (Table S2) recorded in ten replicates each. Venetian-blind cross-validation (ten splits, blind thickness = 1) was employed to ensure that every mixture contributed equally to the validation set. A three-factor SIMPLS model proved optimal.

Processed isotope fractions $n(^{14}N)/n(N)$ and $n(^{15}N)/n(N)$ were inserted into the isotope-dilution equation to obtain the nitrogen mass fraction of the sample, w_{sample} (eqn (1)), where $w_{spike,15N}$ is the ^{15}N mass fraction in the spike, $M_{(sample)}$ and

$M_{(15N)}$ are the molar masses of nitrogen in the sample and spike, respectively, $x_{sample,15N}$ is the amount fraction of ^{15}N in the sample, m denotes the masses of the spike and sample, and R represent the isotope ratios in the spike, sample, and mixed solutions. All uncertainty components, sample and spike weighing, spike characterization, and ratio precision, were calculated using GUM Workbench 2.4 (Metrodata GmbH, Germany) and Open Monte Carlo Engine v1.2.3 (Ruediger Kessel, NIST, USA).

$$w_{sample} = w_{spike,}{}^{15}N \frac{M_{(sample)}}{M_{(^{15}N)}} \times x_{sample,^{15}N} \times \frac{m_{spike}}{m_{sample}} \times \frac{R_{spike} - R_{mix}}{R_{mix} - R_{sample}} \quad (1)$$

The isotope dilution limit of detection (LoD_{ID}) is obtained by propagating the instrumental LoDs of the two isotopes through the ID equation, following the derivation of Yu *et al.*[28] in its simplified form (eqn (2)):

$$LoD_{ID} = \left| \frac{LoD_{^{14}N} - R_{spike}\ LoD_{^{15}N}}{x(^{14}N)_{sample} - R_{spike} x(^{15}N)_{sample}} \right| \quad (2)$$

The numerator represents the smallest measurable difference between the two isotope signals: the LoD for ^{14}N minus the ^{15}N LoD scaled by the spike isotope ratio $R_{spike} = n(^{14}N)/n(^{15}N)$ in the spike solution. The denominator is the sensitivity factor that converts a change in isotope ratio into a change in analyte mass; it is the difference between the natural-abundance ^{14}N atom fraction in the sample $x(^{14}N)_{Sample}$ and the same fraction weighted by the spike ratio. As R_{spike} (*i.e.*, as the spike becomes more ^{15}N-enriched), the denominator grows and the overall LoD_{ID} decreases, reflecting the greater "lever-arm" afforded by a highly enriched spike. Hence, the equation directly links the method detection limit to the individual isotope sensitivities of the instrument and the degree of spike enrichment, showing that an optimally enriched spike minimizes the mass of N that must be detected. The $LoD_{^{14}N} = 4.8$ ng N and the $LoD_{^{15}N} = 3.2$ ng N, yield an overall LoD_{ID} of 4.8 ng N, equivalent to 0.24 mg L^{-1} N for an aliquot of 20 μL injected into the graphite furnace of the HR-CS-AAS instrument.

Despite the ng detection capability, samples were nonetheless diluted or, if necessary, pre-concentrated (see the next section, solid-phase extraction, SPE) so that the final concentration was close to 10 mg L^{-1} N, to match an integrated absorbance of 0.3 s^{-1}. At this signal level, the rotational-vibrational lines of both ^{14}NO and ^{15}NO isotopologues lie well above the baseline yet remain within the linear range of the detector, ensuring a high signal-to-noise ratio required for reliable PLS deconvolution of the entire molecular profile.

2.5 Solid-phase extraction (SPE, optional pre-concentration)

For samples that contain concentrations <10 mg L^{-1} N, nitrate/nitrite was pre-concentrated on a strong-anion-exchange SPE cartridge (Chromabond HR-XA, 200 mg, 6 mL, Macherey-Nagel). The procedure, adapted from Yu *et al.*,[29] was as follows: condition with 5 mL of water; load 10 mL of sample at a flow rate of 1

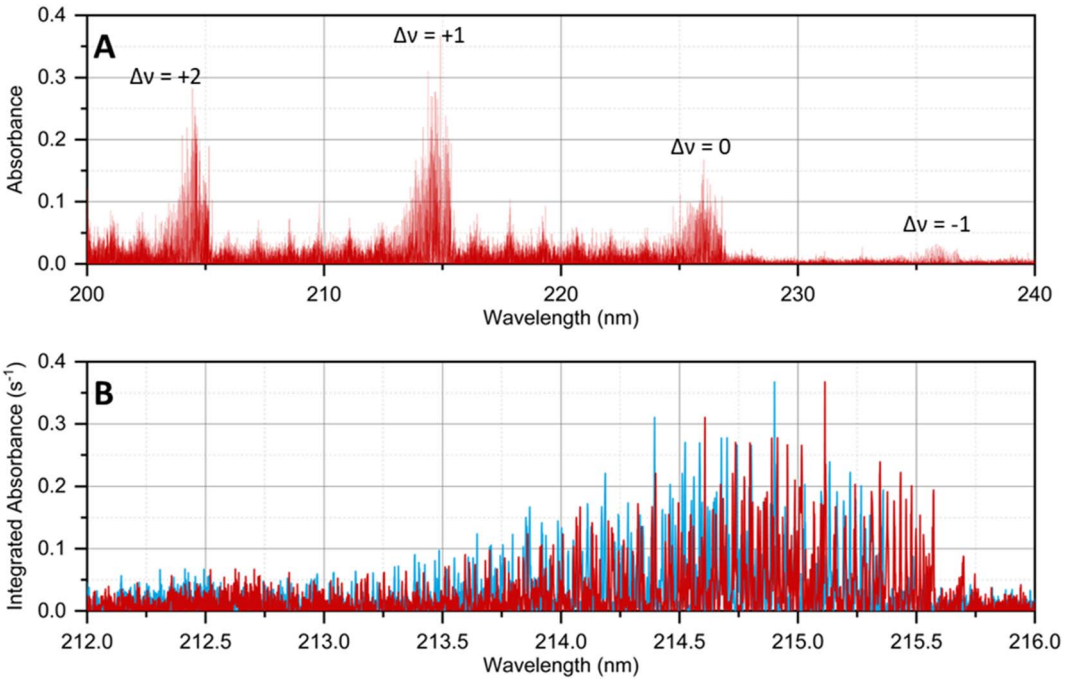

Fig. 1 High-resolution spectra of nitric oxide in the graphite furnace. (A) Overview spectrum (200–240 nm) recorded for NO produced from a 20 μL aliquot of 250 mg L^{-1} N as $^{14}NaNO_3$ plus 5 μL of 1% Ca w v^{-1} modifier. The four vibrational bands of the $A^2\Sigma^+ \leftarrow X^2\Pi$ transition are evident ($\Delta v = +2, +1, 0, -1$); the $\Delta v = +1$ band, centered around 215.3 nm, gives the largest integrated absorbance. (B) Expanded view of the spectral window (212.0–216.0 nm) showing the rotational structure of the $\Delta v = +1$ band for enriched ^{14}NO (blue) and enriched ^{15}NO (red) generated from 100 mg L^{-1} N solutions of $Na^{14}NO_3$ and $Na^{15}NO_3$, respectively.

mL min^{-1}, wash with 2 mL of water, and elute with 1.0 mL of 0.5 mol L^{-1} NH_4Cl. The eluate was spiked gravimetrically with the ^{15}N-nitrate solution, brought to 2.0 mL. A single pass affords 5-fold enrichment with 96 ± 3% recovery, tested with a 0.5 mg L^{-1} N solution in triplicate.

3. Results and discussion

3.1 Generation of NO and furnace optimization

Thermal decomposition of nitrate and nitrite in the graphite furnace produced the characteristic NO spectra for the electronic transition $A^2\Sigma^+ \leftarrow X^2\Pi$. Fig. 1A shows a typical spectrum obtained from 250 mg L^{-1} N (as $NaNO_3$) with a $CaCl_2$ modifier: four vibrational bands ($\Delta v = +2, +1, 0, -1$) are resolved, confirming quantitative conversion of nitrate and nitrite to NO. The band head around 215.3 nm ($\Delta v = +1$) delivered the highest integrated absorbance and was selected for all further work (Fig. 1B).

Furnace-temperature optimization (Fig. S2 and S3) indicated that nitrate decomposed above 350 °C; therefore, the pyrolysis step was fixed at 300 °C. A slow atomization ramp (50 °C s^{-1}) up to 800 °C maximized NO absorbance and ensured a stable molecular signal for isotope ratio analysis, as higher temperatures offered no further gain and risked decomposition. Under these conditions, the blank signal remained stable, providing a robust baseline for isotope-ratio work.

3.2 Matrix tolerance and selectivity

Fig. 2 shows that, at a fixed 5 mM total nitrogen, the summed NO absorbance (1.92 ± 0.09 s^{-1}) is constant as the NO_2^-/NO_3^- ratio moves from 0 : 1 to 1 : 0, proving that both anions are converted to NO with identical efficiency. Fig. S3 confirms equal molar response for the two anions. Consequently, nitrate and nitrite share a single calibration factor on a nitrogen basis, allowing total oxidized nitrogen to be treated as a single analyte.

The matrix tolerance is based directly on the detailed interference studies of Huang *et al.* and Brandao *et al.*[22,23] Huang demonstrated that acids and metal ions can suppress the NO signal; however, low-temperature pyrolysis (≤150 °C) and a Ca modifier largely mitigate this issue. Brandao confirmed the same behavior for nitrite and demonstrated that even 5% HCl suppresses the nitrite-derived NO far more strongly than the nitrate-derived NO, a feature they exploited for speciation. As the current isotope-dilution method measures the ratio of native ^{14}NO to spike ^{15}NO, any residual suppression acts equally on both isotopologues, leaving the calculated concentration unaffected. Therefore, matrix effects are cancelled out by design.

An additional tolerance test (Fig. 3) shows that fluoride, sulfate, and phosphate, added individually at concentrations up to 1000 mg L^{-1}, reduce the NO absorbance by no more than 18%. This minor attenuation indicates that the probable formation of stable $Ca(NO_3)_2$ (and $Ca(NO_2)_2$) effectively retains the analyte even in highly saline waters. Absorption bands of the carbon sulfide (CS) molecule occasionally appear in sulfur-rich matrices. Still, the slow atomization ramp keeps the NO lines temporally separated from the CS absorption lines, preventing overlap (vaporization of NO occurs early than the CS molecule). These results confirm that the ID-HR-CS-GF-MAS method is insensitive to the ionic compositions typically encountered in natural samples, and that no separate reduction/oxidation or matrix-matching steps are required for SI-traceable nitrate/nitrite quantification.

3.3 Isotope shift on the NO isotopologues

Fig. 4 compares the high-resolution spectra of the isotopologues ^{14}NO and ^{15}NO recorded in the $\Delta v = +1$ band head around

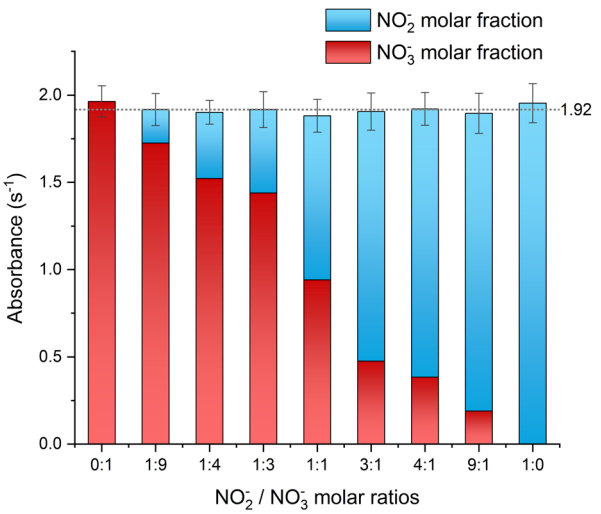

Fig. 2 Total NO absorbance obtained from binary mixtures of nitrate (red) and nitrite (blue) that contain the same total nitrogen concentration (5 mM) but different NO_2^-/NO_3^- molar ratios (0 : 1 to 1 : 0). Error bars represent the mean ± 1 SD of four replicate injections: instrumental settings as in Table S1. The dotted line (1.92 s^{-1}) marks the average integrated absorbance expected for complete and stoichiometric conversion of both anions to NO.

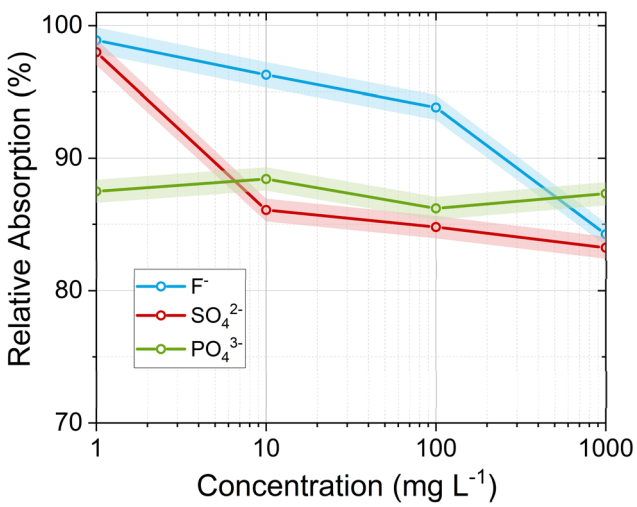

Fig. 3 Influence of fluoride, sulfate, and phosphate ions on the NO signal. Relative integrated absorbance of NO (λ = 215.359 nm) plotted against the concentration (log scale) of fluoride (blue), sulfate (red), and phosphate (green) added to a nitrate standard. Each data point represents a 50 : 50 (v/v) mixture of $NaNO_3$ solution (100 mg L^{-1} N) and an ion solution. Shaded regions denote ±1 SD (n = 4).

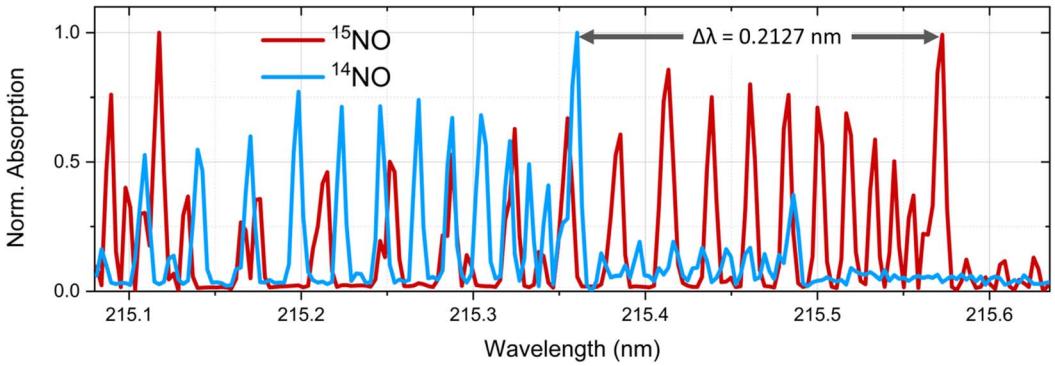

Fig. 4 High-resolution molecular absorption lines of NO isotopologues ^{14}NO and ^{15}NO recorded with HR-CS-GF-MAS in the spectral window around the band head $\Delta v = +1$ at 215 nm. The spectrum for ^{14}NO (blue) was obtained from a 99.9 atom% 14N-enriched sodium nitrate spike solution, whereas the ^{15}NO trace (red) derives from a 98 atom% ^{15}N-enriched sodium nitrate spike (both 100 mg L^{-1} N). Rotational-vibrational lines of the two isotopologues are almost fully resolved; the main features are shifted by 0.2127 nm.

215 nm for the electronic transition $A^2\Sigma^+ \leftarrow X^2\Pi$. Although the two isotopologues share the same electronic transition, every rotational–vibrational line of ^{15}NO is displaced by 0.2127 nm from each other. The shift arises because replacement of ^{14}N (m = 14.0031 u) by the heavier ^{15}N (m = 15.0001 u) increases the reduced mass (μ) of the NO molecule, the rotational constant $B \propto 1/\mu$, and the vibrational term values $G(v) \propto \sqrt{k/\mu}$ therefore decrease (where k is the force constant), pushing all transition energies slightly lower and the wavelengths correspondingly higher. For diatomic molecules, the combined rotational and vibrational mass effects are significantly larger than the purely electronic isotope shifts observed in atomic spectra, making the separation exploitable with an echelle spectrograph operating at $\lambda/\Delta\lambda \approx 140\,000$.

Under the optimized furnace conditions, the rotational lines are sufficiently sharp that the most intense ^{14}NO and ^{15}NO lines are baseline-separated; crosstalk is <0.3% when a 0.020 nm integration window is applied around each peak. This resolution is essential for optical isotope dilution because it allows the absorbances of the two isotopologues to be measured independently and related directly to the ^{15}N/^{14}N amount ratio in the graphite furnace atomization. The 0.2127 nm displacement also agrees with literature data for the γ-system,[30] confirming that the spectrometer's wavelength scale is accurate to better than ±0.002 nm. The matrix-induced line shifts are negligible at the selected atomization temperature.

3.4 Chemometric evaluation and method performance

The NO isotopologues are separated by 0.2127 nm, but their absorption lines partially overlap (see Fig. 1B and 4), preventing them from being treated as independent analytical channels. Consequently, non-linear multivariate analysis is required for spectral deconvolution and determination of isotope ratios. Raw time-resolved spectra were averaged over the atomization pulse, blank-subtracted, area-normalized, converted to a Savitzky–Golay second derivative (11 pt, 4th-order), and mean-centered (Table S3). A calibration space was then built from ten gravimetrically prepared binary mixtures whose ^{15}N/^{14}N amount ratios spanned the full range from 0 to 10 (Table S2). These "ratio standards" were made solely by weighing the enriched $Na^{15}NO_3$ and enriched $Na^{14}NO_3$ salts, so that the isotope fractions are traceable to the SI *via* weighing.

A SIMPLS PLS-R model with three latent variables related the treated spectra (X-block, 215.155–215.450 nm) to the gravimetric isotope fractions $n(^{14}N)/n(N)$ and $n(^{15}N)/n(N)$ (Y-block), the first latent variable (LV1) accounting for 94% of the X-variance and 98% of the Y-variance (overall NO absorbance). LV2 contributed a further 3.5%/1.1% (systematic wavelength shift), and LV3 2%/0.2% (minor baseline differences). Additional latent variables reduced the cross-validated error by <1% and began to fit noise, so the rank was fixed at LV = 3. Cross-validation (venetian blinds, 10 splits) gave the resulting statistics, RMSEC = 5.3‰, RMSECV = 6.2‰, $R_{cal}^2 = 0.999699$, $R_{CV}^2 = 0.999595$, confirming excellent linearity across the full isotopic range. Hotelling-T^2 and Q-residual tests (95% threshold) revealed no outliers. A single prediction of the ^{15}N/^{14}N ratio therefore carries a relative standard uncertainty of approximately 0.3%, which is fully compatible with the 2–4% combined uncertainty targeted for the isotope-dilution measurement.

The concentration of the ^{15}N-spike solution was established by reverse isotope dilution against the NIST SRM 3185 nitrate standard, providing the link to the primary SI traceability chain. In this approach, a known amount of certified standard is mixed with the spike solution, and the resulting isotope ratio is measured. By rearranging the ID equation and inserting the certified mass fraction of the standard, the unknown spike concentration can be calculated.[31] Once the spike concentration was known, unknown samples were spiked, measured, and the PLS-R predicted isotope fractions were inserted into the ID equation (eqn (1)) to obtain the nitrate-equivalent nitrogen mass fraction.

Accuracy was verified with four certified reference materials (CRM concentrations 2.9–1000 mg L^{-1} NO_3^-). For each material, the E_n value was calculated: the absolute difference between the measured value and the certificate, normalized by the combined (expanded) uncertainty of that difference.[32] An E_n less than one signals agreement, whereas values above one indicate incompatibility. In many cases, E_n remained below

unity, and the corresponding expanded uncertainties ($k = 2$) were only 2–4%. For the spike-to-sample ratios where the calculated $|E_n|$ exceeded the unity, these correspond to highly unbalanced isotope ratios, where the ID equation is most sensitive to small deviations in the measured 15N/14N value or to the relatively large uncertainty quoted for the low-level CRMs. When the spike and sample were brought close to the equimolar ratio ($\approx 50:50$), almost all materials showed $|E_n| < 1$, confirming the absence of a systematic bias and highlighting the importance of an optimized spike/sample match for the lowest uncertainty.

So, the optimum precision (average $U_{rel} \approx 1.2\%$) occurred at $^{15}N:^{14}N \approx 1$, the ratio targeted in routine analyses. Finally, twenty Berlin surface-water samples were analyzed the same way, demonstrating that the spectroscopic isotope dilution method—grounded in gravimetry, powered by spectral deconvolution and anchored by a NIST-traceable spike—delivers reliable, SI-traceable nitrate/nitrite concentrations in real environmental matrices.

Fig. S1 summarizes the workflow for analysis by ID-HR-CS-MAS. Instrumental limits of detection were 4.80 ng (^{14}N) and 3.15 ng (^{15}N). Applying the symmetric ID-LoD expression gave a combined method LoD of 21.05 ng NO_3^- (0.24 ng N) per 20 μL injection.

3.5 Application to Berlin surface waters

Berlin's water supply relies heavily on the river-lake network of the Spree and upper Havel, a system already strained by low natural runoff, declining mine-water discharges, and intense agricultural and industrial demands. Because 74% of the city's drinking water is produced by bank filtration or artificial recharge of surface water—compared with a national German average of 16%—any accumulation of oxidized nitrogen is of particular concern.[33]

Twenty sites were sampled in early April 2025 (Table 2 and Fig. 5). Total nitrate and nitrite (reported as nitrate equivalent NO_3^-) spanned more than two orders of magnitude, from 0.10 mg L^{-1} in the outer Spree to 7.3 mg L^{-1} in the inner-city Panke. Main reaches of the Spree, Dahme and Havel remained below 0.8 mg L^{-1} NO_3^-, reflecting effective dilution and limited upstream agriculture. Two corridors showed pronounced enrichment:

(a) Teltow canal. Concentrations rose steadily from 2.5 mg L^{-1} NO_3^- at Adlershof to 4.7 mg L^{-1} NO_3^- at Kleinmachnow, mirroring inputs of treated municipal wastewater.

(b) Panke river. A maximum of 7.3 mg L^{-1} NO_3^- at Schönwalder Straβe confirms this small tributary as a disproportionate nitrogen source to the Spree.

Even the highest values remain well below the EU drinking-water limit of 50 mg L^{-1} NO_3^- (≈ 10 mg L^{-1} N).[4] Yet, local eutrophication is likely in sluggish canal sections where hydraulic residence times are long.[34] The spatial distribution agrees with mass-balance estimates from earlier studies,[35–37] demonstrating that ID-HR-CS-GF-MAS can deliver rapid, SI-traceable snapshots of urban nitrogen loads.

Compared with routine ion chromatography[7] (LoD 5–23 μg L^{-1} N for NO_3^- and NO_2^-, respectively) and classical ID-MS[9] (LoD $\approx$ 0.03 μg L^{-1} N but ≥20 min per run), the optical ID method offers ng sensitivity, direct SI traceability without mass-spectrometric infrastructure, and a total cycle time of a few minutes. Capital expenditure is far lower than for an ID-MS system, making the technique attractive for routine surveillance and for certifying reference materials when rapid, absolute quantification is required.

Table 2 Total NO_3^- equivalent concentrations determined by ID-HR-CS-GFMAS at 20 fluvial and canal sites sampled between April 3 to 5, 2025. The expanded uncertainties are expressed at the 95% confidence level ($k = 2$)

	Place	NO_3^- equiv./mg L^{-1}	U	N/μg L^{-1}	U	Geographical coordinates
1	Langer see – Bammelecke	0.80	±0.04	180.67	±0.06	52°24′27.9″N 13°37′19.2″E
2	Spree – Spreetunnel	0.190	±0.010	42.91	±0.02	52°26′39.7″N 13°37′30.0″E
3	Dahme – Teltowkanal	0.79	±0.04	158.09	±0.06	52°25′39.7″N 13°34′31.3″E
4	Teltowkanal – Adlershof	2.5	±0.2	564.60	±0.20	52°25′32.6″N 13°32′09.8″E
5	Teltowkanal – Buschkrugbrücke	2.8	±0.2	632.35	±0.22	52°27′34.2″N 13°26′50.6″E
6	Teltowkanal – Hafen Steglitz	2.25	±0.13	496.84	±0.17	52°26′36.2″N 13°19′32.8″E
7	Teltowkanal – Eugen-Kleine-Brücke	2.83	±0.17	632.35	±0.22	52°25′11.3″N 13°18′09.1″E
8	Teltowkanal – Kleinmachnow	4.7	±0.3	1061.44	±0.37	52°23′58.8″N 13°10′45.6″E
9	Spree – Fähre Baumschulenweg	0.16	±0.01	36.13	±0.01	52°28′20.1″N 13°29′42.3″E
10	Spree – Lohmühleninsel	0.56	±0.03	126.47	±0.04	52°29′49.5″N 13°27′24.3″E
11	Spree – Jannowitzbrücke	0.39	±0.05	171.64	±0.06	52°29′51.1″N 13°23′32.5″E
12	Landwehrkanal – Hallesches-Tor-Brücke – Kreuzberg	0.77	±0.015	67.75	±0.02	52°30′48.4″N 13°25′10.4″E
13	Panke – Schönwalder Straβe	7.3	±0.4	1648.62	±0.58	52°32′33.1″N 13°22′24.3″E
14	Spree – Landwehrkanal	0.77	±0.04	173.90	±0.06	52°31′13.5″N 13°19′04.3″E
15	Hohenzollernkanal – Schleuse Plötzensee	1.80	±0.10	406.51	±0.14	52°32′43.5″N 13°19′17.3″E
16	Westhafenkanal – Mörschbrücke	1.00	±0.06	225.84	±0.08	52°31′56.2″N 13°17′40.0″E
17	Spree – Sophienwerder	0.110	±0.011	24.84	±0.01	52°32′10.1″N 13°12′57.3″E
18	Havel – Stößenseebrücke	1.6	±0.1	361.34	±0.13	52°30′34.2″N 13°12′54.0″E
19	Havel – Grunewaldturm	1.39	±0.08	293.59	±0.10	52°28′41.7″N 13°11′29.1″E
20	Wannsee – Pfaueninsel	1.30	±0.08	293.59	±0.10	52°25′44.9″N 13°07′18.2″E

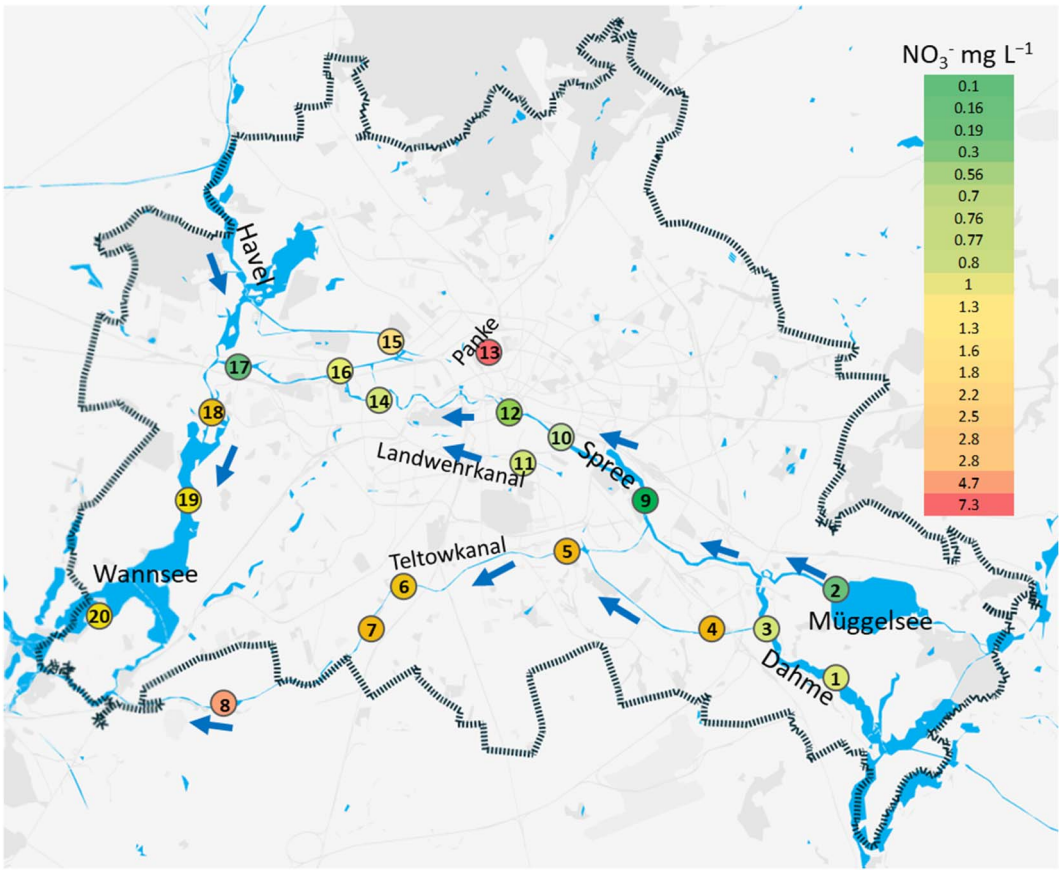

Fig. 5 Spatial distribution of dissolved total NO_3^- equivalent in Berlin surface waters from April 3 to 5, 2025. Circles mark the 20 sampling locations analyzed by ID-HR-CS-GF-MAS; colors follow the logarithmic legend at upper right (green = 0.10 mg L^{-1} N, red = 7.3 mg L^{-1} N). Blue arrows indicate principal flow directions of the major water bodies (© Google Maps).

Thus, by resolving the 0.2127 nm isotopic shift of NO and coupling it with isotope dilution, HR-CS-GF-MAS provides an accurate, robust and economical route to total-nitrate/nitrite data—precisely the kind of high-quality information needed to safeguard surface-water-dominated drinking-water supply under increasing hydrological pressure.

4. Conclusion

This work confirms that isotope-dilution high-resolution continuum-source graphite furnace molecular-absorption spectrometry (ID-HR-CS-GF-MAS) can provide a primary, calibration-free route to total nitrate + nitrite in natural waters. By resolving the 0.213 nm isotopic shift between ^{14}NO and ^{15}NO isotopologues, the spectrometer furnishes a direct optical measurement of the $^{15}N/^{14}N$ amount ratio after a single furnace cycle; when that ratio is combined with a gravimetrically characterized, NIST-traceable ^{15}N spike and a three-latent-variable SIMPLS model, the result is an SI-linked concentration with 2–4% expanded uncertainty. Instrumental limits of detection—4.80 ng (^{14}N) and 3.15 ng (^{15}N)—propagate to a method LoD of 4.75 ng N (≈0.24 mg L^{-1} N for a 20 μL aliquot). The furnace program allows for additional drying/pyrolysis loops, enabling the layering of extra 20 μL portions on the platform, and single-pass SPE steps afford nitrate/nitrite enrichment, pushing the practical detection limit well into the μg L^{-1} regime.

Four certified reference materials spanning three orders of magnitude were metrologically compatible ($|E_n| < 1$) across a range of spike-to-sample ratios, and twenty Berlin surface-water samples yielded concentrations from 0.10 to 7.3 mg L^{-1} NO_3^--equivalent, faithfully reproducing known spatial patterns and identifying the Panke River and Teltow Canal as dominant nitrogen sources. Matrix studies indicate that common freshwater anions and mixed NO_2^-/NO_3^- compositions exert only minor attenuation, which cancels out in the isotope-ratio measurement; therefore, no matrix matching or redox pretreatment is required.

Although the proof-of-concept already meets regulatory needs, several refinements will further strengthen the metrology and potentially be used for precise isotope amount ratio analysis. Re-determining the ^{14}N and ^{15}N salt atom fractions using high-precision ID-MS, incorporating more PLS-R training mixtures with additional isotope ratios, and testing extreme salinities or high organic loads will all enhance accuracy and robustness. A mixed-isotope check standard would provide routine performance control and facilitate long-term validation. At the same time, systematic studies of tube memory during multi-aliquot stacking will secure the ultra-

trace region now accessible through on-platform enrichment or SPE.

None of these practical considerations detracts from the central outcome: optical isotope dilution, implemented with HR-CS-GF-MAS, delivers ID-MS-level accuracy in a fraction of the time and at a fraction of the cost. By combining the intrinsic accuracy and precision of isotope dilution with the operational simplicity of molecular absorption spectroscopy, the method provides an attractive, SI-traceable alternative for routine nitrate/nitrite surveillance, reference material production, and, in the future, the absolute quantification of other light-element species whose isotopologues are within the reach of high-resolution continuum-source spectrometry. While the current chemometric processing requires expert-level data handling, this work establishes a foundation for implementing SI-traceable isotope dilution workflows in commercial instruments through dedicated software development, potentially enabling broader adoption of optical ID techniques.

Conflicts of interest

There are no conflicts of interest to declare. The systems used – MOSES and contrAA 800 – were developed and provided by Analytik Jena GmbH.

Data availability

Additional data supporting this article have been included as part of the SI.

SI contains furnace-optimisation data, calibration-mixture compositions, detailed heating programme, chemometric parameters, and additional figures supporting method validation and performance. See DOI: **https://doi.org/10.1039/d5ja00252d**.

Acknowledgements

The authors are grateful to Dr Jochen Vogl (BAM, Division Inorganic Trace Analysis) for his constructive comments, which helped to improve this study, and to Analytik Jena GmbH for their support in this research.

References

1 V. H. Smith, G. D. Tilman and J. C. Nekola, *Environ. Pollut.*, 1999, **100**, 179–196.
2 S. Khademikia, Z. Rafiee, M. M. Amin, P. Poursafa, M. Mansourian and A. Modaberi, *J. Environ. Public Health*, 2013, **2013**, 603468.
3 United States Environmental Protection Agency, *Maximum Contaminant Levels for Inorganic Contaminants, 40 CFR § 141.62*, 2025.
4 Council of the European Communities, *Concerning the protection of waters against pollution caused by nitrates from agricultural sources, Council Directive 91/676/EEC*, 1991.
5 X. Desmit, V. Thieu, G. Billen, F. Campuzano, V. Dulière, J. Garnier, L. Lassaletta, A. Ménesguen, R. Neves, L. Pinto, M. Silvestre, J. L. Sobrinho and G. Lacroix, *Sci. Total Environ.*, 2018, **635**, 1444–1466.
6 D. V. Chapman and T. Sullivan, *One Earth*, 2022, **5**, 132–137.
7 J. A. Morales, L. S. de Graterol and J. Mesa, *J. Chromatogr., A*, 2000, **884**, 185–190.
8 X. Du, S. Ye and D. Dong, *J. Food Process. Eng.*, 2019, **42**, e13164.
9 J.-C. Wolff, P. D. P. Taylor and P. De Bièvre, *Anal. Chem.*, 1996, **68**, 3231–3237.
10 E. Pagliano, J. Meija and Z. Mester, *Anal. Chim. Acta*, 2014, **824**, 36–41.
11 B. Welz, H. Becker-Ross, S. Florek and U. Heitmann, *High-Resolution Continuum Source AAS: the Better Way to Do Atomic Absorption Spectrometry*, Wiley-VCH Verlag GmbH & Co. KGaA, 2006.
12 F. V. Nakadi, M. A. M. S. da Veiga, M. Aramendía, E. García-Ruiz and M. Resano, *J. Anal. At. Spectrom.*, 2015, **30**, 1531–1540.
13 F. V. Nakadi, M. A. M. S. da Veiga, M. Aramendia, E. Garcia-Ruiz and M. Resano, *J. Anal. At. Spectrom.*, 2016, **31**, 1381–1390.
14 M. B. T. Zanatta, F. V. Nakadi, M. Resano and M. A. M. S. da Veiga, *J. Anal. At. Spectrom.*, 2019, **34**, 2280–2287.
15 A. Bazo, R. Garde, E. Garcia-Ruiz, M. Aramendía, F. V. Nakadi and M. Resano, *J. Anal. At. Spectrom.*, 2022, **37**, 2517–2528.
16 M. Aramendía, A. L. M. de Souza, F. V. Nakadi and M. Resano, *J. Anal. At. Spectrom.*, 2024, **39**, 767–779.
17 A. Winckelmann, D. Morcillo, S. Richter, S. Recknagel, J. Riedel, J. Vogl, U. Panne and C. Abad, *Anal. Bioanal. Chem.*, 2022, **414**, 251–256.
18 C. Abad, S. Florek, H. Becker-Ross, M.-D. Huang, H.-J. Heinrich, S. Recknagel, J. Vogl, N. Jakubowski and U. Panne, *Spectrochim. Acta, Part B*, 2017, **136**, 116–122.
19 A. Winckelmann, S. Nowak, S. Richter, S. Recknagel, J. Riedel, J. Vogl, U. Panne and C. Abad, *Anal. Chem.*, 2021, **93**, 10022–10030.
20 D. Morcillo, A. Winckelmann, D. A. Frick, L. Jacobsen, T. Seger, S. Florek, S. Richter, J. Vogl, S. Recknagel, U. Panne and C. Abad, *Spectrochim. Acta, Part B*, 2024, **220**, 107013.
21 G. Herzberg, *Molecular Spectra and Molecular Structure I. Spectra of Diatomic Molecules*, Van Nostrand Reinhold, New York, 2nd edn, 1950.
22 M.-D. Huang, H. Becker-Ross, S. Florek, U. Heitmann, M. Okruss, B. Welz and H. S. Ferreira, *J. Anal. At. Spectrom.*, 2010, **25**, 163–168.
23 G. C. Brandao, G. D. Matos, R. N. Pereira and S. L. Ferreira, *Anal. Chim. Acta*, 2014, **806**, 101–106.
24 G. C. Brandao, D. C. Lima and S. L. C. Ferreira, *Talanta*, 2012, **98**, 231–235.
25 P. De Bièvre and H. S. Peiser, *Fresenius. J. Anal. Chem.*, 1997, **359**, 523–525.
26 S. Geisler, M. Okruss, H. Becker-Ross, M. D. Huang, N. Esser and S. Florek, *Spectrochim. Acta, Part B*, 2015, **107**, 11–16.
27 Z. Kowalewska, C. Abad, M. Okruss and S. Recknagel, *J. Anal. At. Spectrom.*, 2023, **38**, 472.

28 L. L. Yu, J. D. Fassett and W. F. Guthrie, *Anal. Chem.*, 2002, **74**, 3887–3891.
29 T.-H. Yu, S.-P. Hsieh, C.-M. Su, F.-J. Huang, C.-C. Hung and L.-M. Yiin, *Int. J. Anal. Chem.*, 2018, **2018**, 6285867.
30 J. Danielak, U. Domin, R. Ke, M. Rytel and M. Zachwieja, *J. Mol. Spectrosc.*, 1997, **181**, 394–402.
31 J. Vogl and W. Pritzkow, *MAPAN*, 2010, **25**, 135–164.
32 J. Vogl, M. Rosner, S. A. Kasemann, R. Kraft, A. Meixner, J. Noordmann, S. Rabb, O. Rienitz, J. A. Schuessler, M. Tatzel and R. D. Vocke, *Geostand. Geoanal. Res.*, 2020, **44**, 439–457.
33 I. Pohle, S. Zeilfelder, J. Birner and B. Creutzfeldt, *Nat. Hazards Earth Syst. Sci.*, 2025, **25**, 1293–1313.
34 M. Geupel, J. Heldstab, B. Schäppi, J. Reutimann, M. Bach, U. Häußermann, L. Knoll, L. Klement and L. Breuer, *Sustainability*, 2021, **13**, 1121.
35 I. Schauser, I. Chorus and J. Lewandowski, *Acta Hydroch. Hydrob.*, 2006, **34**, 325–332.
36 G. Massmann, J. Sültenfuß, U. Dünnbier, A. Knappe, T. Taute and A. Pekdeger, *Hydrol. Process.*, 2008, **22**, 788–801.
37 F. Ortmeyer, B. Hansen and A. Banning, *Grundwasser*, 2023, **28**, 3–22.